

# Assisted Physical Interaction: Autonomous Aerial Robots with Neural Network Detection, Navigation, and Safety Layers

Andrea Berra<sup>\*1</sup>, Viswa Narayanan Sankaranarayanan<sup>\*2</sup>, Achilleas Santi Seisa<sup>\*2</sup>, Julien Mellet<sup>\*3</sup>, Udayanga G.W.K.N. Gamage<sup>\*4</sup>, Sumeet Gajanan Satpute<sup>2</sup>, Fabio Ruggiero<sup>3</sup>, Vincenzo Lippiello<sup>3</sup>, Silvia Tolu<sup>4</sup>, Matteo Fumagalli<sup>4</sup>, George Nikolakopoulos<sup>2</sup>, Miguel Ángel Trujillo Soto<sup>1</sup>, and Guillermo Heredia<sup>5</sup>

**Abstract**—The paper introduces a novel framework for safe and autonomous aerial physical interaction in industrial settings. It comprises two main components: a neural network-based target detection system enhanced with edge computing for reduced onboard computational load, and a control barrier function (CBF)-based controller for safe and precise maneuvering. The target detection system is trained on a dataset under challenging visual conditions and evaluated for accuracy across various unseen data with changing lighting conditions. Depth features are utilized for target pose estimation, with the entire detection framework offloaded into low-latency edge computing. The CBF-based controller enables the UAV to converge safely to the target for precise contact. Simulated evaluations of both the controller and target detection are presented, alongside an analysis of real-world detection performance.

**Index Terms**—Aerial Physical Interaction; UAVs; Control Barrier Function; Neural Network; Edge Computing.

## I. INTRODUCTION

Operating Micro Aerial Vehicle (MAV)s for inspections and maintenance is crucial in industries, as demonstrated in projects such as ARCAS and AEROARMS [1]. It is particularly pertinent in hazardous and hard-to-reach environments. Autonomous Unmanned Aerial Vehicle (UAV)s have improved reliability and safety, especially in the absence of Line of Sight (LoS) [2]. Subsequently, aerial manipulation has become a rapidly growing area of research, offering interesting challenges in the Point-of-Interest (PoI) localization and ensuring safe navigation, while incorporating diverse robotic systems for autonomous Aerial Physical Interaction (APhI) with the environment [3]. Since UAVs with their razor-sharp propellers can wreak havoc during a crash, it is essential to ensure security at different levels. Conventional

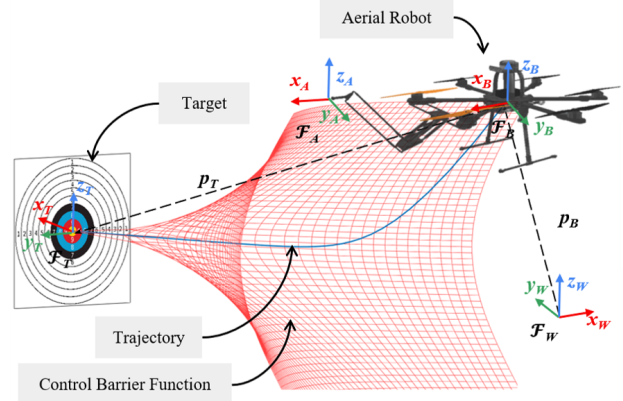


Fig. 1: Schematic of the boundary of the control barrier function, which guides the aerial platform’s trajectory to reach the target precisely.

methods often entail the use of an expert operator [4], necessitating complete supervision combined with high mental demand. On the other hand, autonomous vehicles running fully onboard often lack safety features and are prompted by unexpected technical limitations.

Motivated by the consistent need for advanced safety for autonomous APhI, this work aims to develop a pipeline for PoI localization and establish precise and safe contact with it. Further, we seek to enhance the performance using a neural-based target detection strategy, coupled with edge computing. To validate the proposed methodology, a realistic simulation incorporating an aerial manipulator and its surrounding environment is proposed. The simulated UAV encompasses the aerial manipulator platform developed for experimental phases, coupled with the sensor setup and diverse simulated world environments. The inclusion of different world environments allows us to robustly evaluate the proposed approach under different environmental conditions.

### A. Related Work

Neural networks have made significant advancements in target detection, especially in challenging UAV image processing environments. Applications include precision agriculture for fruit classification [5], maritime surveillance [6], forest fire detection [7], and search and rescue operations [8]. The widely used You Only Look Once (YOLO) network [9] is prevalent in aerial target detection due to its reliable performance and improved accuracy, reaching centimeter-

This project has received funding from the European Union’s Horizon 2020 research and innovation program under the Marie Skłodowska-Curie grant agreement No 953454.

<sup>1</sup>CATEC, Advanced Center for Aerospace Technologies, Seville, Spain.

<sup>2</sup>Robotics and AI Team, Department of Computer, Electrical and Space Engineering, Luleå University of Technology, Luleå, Sweden.

<sup>3</sup>PRISMA Lab, Department of Electrical Engineering and Information Technology, University of Naples Federico II Naples, Italy.

<sup>4</sup>Automation and Control Group, Department of Electrical Engineering and Photonics, Technical University of Denmark, Denmark.

<sup>5</sup>Robotics, Vision, and Control Group School of Engineering, University of Seville, Seville, Spain.

\*The authors contributed equally

Corresponding Authors’ email: {vissan, achsei}@ltu.se, aberra@catec.aero, julien.mellet@unina.it, kniud@dtu.dk

level precision in UAV applications [10]. Tailored adaptations of YOLO for UAV imagery conditions, such as occlusion and brightness variations, have also been proposed [11].

However, many existing approaches require substantial computational resources beyond what is available on UAV onboard computers. Edge computing has emerged as a crucial solution for computational offloading, offering superior computational power compared to onboard systems and reduced latency relative to cloud computing. For example, in [12], a lightweight object recognition algorithm based on You Look Less than Once (YLLO) runs on the edge for real-time traffic area monitoring with minimal data to preserve accuracy. Similarly, in [13], edge computing supports real-time object identification and classification by multiple aerial and mobile robots using a YOLO algorithm.

Safety and precision in aerial robotic systems have been approached from a Prescribed Performance Control (PPC) perspective [14]–[16]. While PPC ensures safety, it typically requires an external planner. However, recent advancements in Control Barrier Function (CBF) offer an elegant solution for providing safety in dynamic systems without the need for an external planner [17]. CBFs linearize constraints over the control space, making it suitable for navigation applications to run directly on the onboard computer.

In this context, while neural networks have shown promise for end-to-end control [18], our approach focuses on leveraging model-based control for safety, providing a continuous definition of the output controller with a dynamic model [19]. Although neural-based techniques excel in image processing tasks [20], we opt to use them solely for detection purposes in our autonomous system. We complement this approach by offloading to edge computing platforms. While CBFs have been utilized in aerial robots for collision avoidance [21] and landing [22], their application for actively enforcing safe navigation to establish physical contact is novel and unexplored. While [23], [24] have proposed CBF approaches for physical interaction using a manipulator, they have been used in the context of avoidance. Similarly, [25] proposes a CBF approach for aerial interaction to improve the tracking efficiency for uncertainties. When it comes to APhI, the need is to precisely enable contact at a given point, while avoiding collision with the target. The CBF used in this approach guides the UAV to achieve this without an external planner.

### B. Contributions

Given the identified shortcomings, our contributions encompass 1) the design of a dataset for computer vision adapted to the uncertainties of industrial environments; 2) including edge computing for data processing; 3) ensuring safe navigation and precise contact using a novel CBF; and 4) qualitative evaluation of the proposed system in some demanding conditions.

## II. METHODOLOGY

Our proposed pipeline comprises three main components: robot localization, PoI or target localization, and safe navigation. The robot localization and navigation modules run

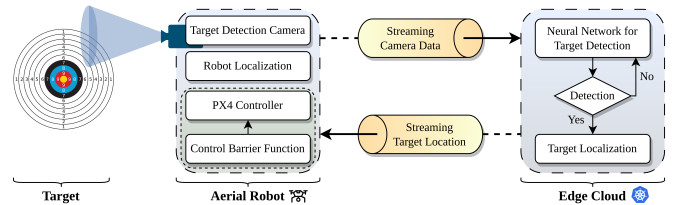


Fig. 2: Schematic of the architecture incorporating edge offloading for the target detection and localization.

onboard, while the computationally heavy target localization runs offboard on an edge computer (see Fig. 2). Additionally, a simulation environment is developed to replicate the real setup for testing and remote visualization purposes. The following subsections provide a detailed discussion of each component.

### A. Robot Localization

A crucial aspect of autonomous navigation is accurately localizing the platform [26], [27], which involves determining its pose relative to a fixed frame. However, traditional methods relying solely on Global Navigation Satellite System (GNSS) can be unreliable in metallic or underground environments. Hence, alternative methods such as Visual Inertial Odometry (VIO) become indispensable.

In this work, we use RGBD-camera-based VIO with the vehicle’s onboard Inertial Measurement Unit (IMU) for estimating the UAV’s pose [28]. We further improve the inaccuracies on altitude measurement using a single point micro Light Detection and Ranging (LiDaR) (see Fig. 3).

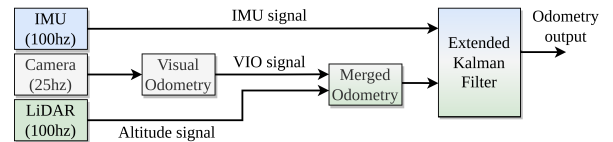
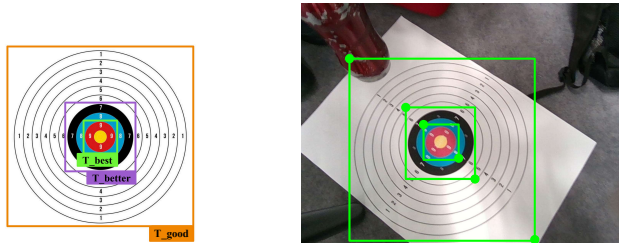


Fig. 3: Block diagram illustrating the VIO localization process, incorporating Visual Odometry, a micro LiDaR sensor, and inertial measurements from the vehicle’s IMU.

In addition, it is essential to determine both the pose of the manipulator’s end-effector and the target’s pose, defined by the frames  $\mathcal{F}_A$  and  $\mathcal{F}_T$ , respectively (see Fig. 1), as well as the pose of two cameras (odometry and target detection camera), relative to the UAV’s body frame, referred to as  $\mathcal{F}_B$ . Hence, all the necessary transformations should be considered. This is crucial for enabling autonomous navigation and precise targeting of the object.

### B. Dataset Design

Fiducial marker detection and localization is a solved problem [29] in a controlled environment without occlusion. Nevertheless, the detection of a custom target with a Red Green Blue (RGB) camera is still challenging. Variations in lighting conditions, background clutter, occlusions, and other factors make traditional algorithms unreliable for safe deployment. While traditional computer vision techniques can lack adaptability [20], neural networks are capable of



(a) Labels associated to target detection levels

(b) Labeling process from *labelme* software [30]

Fig. 4: Image labels for target detection.

learning from diverse data, making them robust to changes. We present our strategy to make a dataset ensuring safe target detection in an industrial context, that is later used to train a convolutional network.

We first define different levels of interest for the target (see Fig 4), allowing accurate target detection at different distances. In our case, we defined three levels: 1)  $T\_good$  is the largest target circumscribing the following two, 2)  $T\_better$  is the intermediate one, surrounding the black circle, and 3)  $T\_best$  is the most accurate feature of the target, including only the two circles that make up the center of the target. We labeled the training set, as presented in Fig. 4a, while Fig. 4b presents the view from *labelme* software [30].

We prepared a dataset of 322 labeled images. We first extracted 18 images from an early flight test in a controlled laboratory environment. We increased the noise in the dataset with 146 images providing obstruction, target surface distortion, various target orientations, and short distance (Figs. 5c, 5d, 5f, 5h). Then, to increase the robustness of the target detection in specific demanding conditions, we fine-tuned the network using on-site data. We thus included 43 images taken from a parking lot, adding blur and long-distance images (Figs. 5a, 5e). We also included 20 images taken on a bright day. The last demanding environment we obtained images from is a tunnel, with 48 images in low-light conditions and flares on the camera (Figs. 5b, 5g). We completed the dataset with 47 images from the simulator. We thus propose a rich dataset with various environmental conditions corresponding to the specific industrial contexts.

We trained the YOLO [9] object detector using the aforementioned dataset. The detected target information is passed to the Target Localization as a bounding box.

### C. Target Localization

Target localization consists of estimating the target object pose from the camera frame using information both from the depth sensor and the color camera. The presented approach involves the estimation of the rotation and translation matrix



(a) Blur

(b) Low light

(c) Obstruction

(d) Distortion

(e) Far

(f) Orientation

(g) Flare

(h) Close

Fig. 5: Samples from the dataset, compiling the environmental variables introduced to add noise.

that solves the difference between the 3D points of the point cloud and the 2D points projected into the camera frame  $\mathcal{F}_C$ , as illustrated in Fig. 6. The solution to the problem, presented here, follows the Perspective-n-Points (PnP) approach introduced in [31],

$$\begin{bmatrix} u \\ v \\ 1 \end{bmatrix} = \begin{bmatrix} f_x & 0 & c_x \\ 0 & f_y & c_y \\ 0 & 0 & 1 \end{bmatrix} \begin{bmatrix} 1 & 0 & 0 & 0 \\ 0 & 1 & 0 & 0 \\ 0 & 0 & 0 & 1 \end{bmatrix} \begin{bmatrix} \mathbf{R}_T^C & p_T^C \\ 0 & 1 \end{bmatrix} \tilde{p}_T^T \quad (1)$$

where  $p_T^C \in \mathbb{R}^3$  and  $R_T^C \in \mathbb{R}^{3 \times 3}$  represents respectively the position and the rotation matrix of the target with respect to the camera frame,  $\tilde{p}_T^T \in \mathbb{R}^4$  indicates a homogeneous representation of target position with respect to camera frame,  $u$  and  $v$  are the coordinates of points projected in image 2D frame, and  $f_x, f_y, c_x, c_y$  are camera known-parameters. Equation (1) establishes the correlation between 2D points observed by the camera and the corresponding 3D coordinates representing the target. Consequently,  $\tilde{p}_T^T$  can be determined by executing the inverse operation in (1).

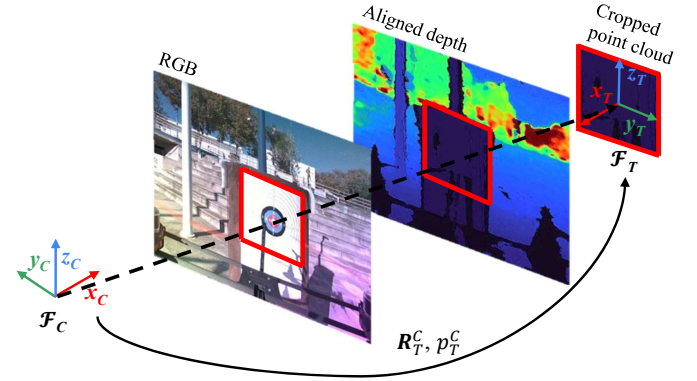


Fig. 6: Estimation of position  $p_T^C$  and orientation  $R_T^C$  of the target frame described by the cropped point cloud.

### D. Platform Description and Control Design

The aerial manipulator platform can be modeled using decoupled dynamics for the UAV and the manipulator. The decoupling simplifies the control strategy. The model of the platform is given by

$$m\ddot{p}(t) + mG = F_p + F_{ext}, \quad (2a)$$

$$\mathbf{J}(q(t))\ddot{q}(t) + \mathbf{C}(q, \dot{q}, t)\dot{q}(t) = \tau_q + \tau_{ext}, \quad (2b)$$

$$\mathbf{M}_A \dot{v}_A^A + \mathbf{D}_A v_A^A + \mathbf{K}_A p_A = -F_A, \quad (2c)$$

where  $p(t) \triangleq [x(t), y(t), z(t)]^T \in \mathbb{R}^3$ ,  $q(t) \triangleq [\phi(t), \theta(t), \psi(t)]^T$  represents the position and orientation of the UAV in the inertial frame ( $\mathbf{X}_W - \mathbf{Y}_W - \mathbf{Z}_W$ );  $G \triangleq [0, 0, -g]^T \in \mathbb{R}^3$  is the gravity vector with  $g = 9.81ms^{-2}$  is

the acceleration due to gravity;  $m, \mathbf{J}, \mathbf{C}$  are the mass inertia and Coriolis matrices of the UAV;  $\tau_q \in \mathbb{R}^3$  is the attitude control input,  $F_{ext}, \tau_{ext}$  are the external force and moment acting on the UAV from the manipulator,  $p_A, v_A$  are the position and linear velocity of the manipulator respectively,  $F_A$  represents the reaction forces on the end-effector, and  $\mathbf{M}_A, \mathbf{D}_A, \mathbf{K}_A$  represent the inertia, damping and elasticity of mechanism. In this work, we consider the manipulator to be unactuated. The only external force acting on the end-effector will be due to the reaction forces from the physical interaction. For further details about the aerial manipulator design, please refer to [32].

We further divide the control framework into position, velocity, and attitude control layers to simply the control design and introduce the safety functionality through CBF. The CBF is used in the position controller to precisely establish contact with the target. Further, it prevents the UAV from deviating or colliding with the target forcefully. In this layer, a pseudo-velocity input is generated

$$u_W = \mathbf{K}_p(p_d - p), \quad (3)$$

where  $\mathbf{K}_p$  is a positive definite gain matrix. This pseudo-velocity input is filtered using a CBF layer to produce the actual velocity input  $u_W^*$ .

The CBF is designed to be a funnel-like function, which converges at the point of contact, as shown in Fig 1. Since velocity input is used in the position dynamics, the model is simplified to the following kinematic equation,

$$\dot{p} = u. \quad (4)$$

The CBF function in this case is designed using a parabolic function, given by

$$h = x_D^T - a\sqrt{l}, \quad (5)$$

where  $x_D^T, y_D^T, z_D^T$  are the location of the UAV with respect to the target frame,  $l = \sqrt{y_D^{T^2} + z_D^{T^2}}$  and  $a$  is a design parameter for reshaping the CBF boundary. The derivatives of the CBF with respect to the states are given by

$$\frac{\partial h}{\partial x_D^T} = 1, \quad \frac{\partial h}{\partial y_D^T} = -\frac{ay_D^T}{2l^{3/4}}, \quad \frac{\partial h}{\partial z_D^T} = -\frac{az_D^T}{2l^{3/4}}. \quad (6)$$

By the CBF definition in [17], the candidate CBF restricts the UAV to operate only in the safe set and precisely establish contact with the target from any initial condition. The CBF constraint is used in the following quadratic equation to generate the velocity input, which ensures safety with only a minimal deviation from the pseudo velocity input,

$$u_T^* = \arg \min_u \|(u - u_T)\| \quad (7)$$

$$\text{s.t. } \frac{\partial h}{\partial p_D^T}(f(x) + g(x)u) \geq -\omega(h) \quad (8)$$

where  $\omega(h)$  is the optimization variable,  $u_T = \mathbf{R}u_W$  is the nominal velocity input in target frame,  $\mathbf{R}$  is the rotation matrix between world frame and target frame,  $\frac{\partial h(\mathbf{p}_D^T, t)}{\partial t} =$

$[\frac{\partial h}{\partial x_D^T} \quad \frac{\partial h}{\partial y_D^T} \quad \frac{\partial h}{\partial z_D^T}]^T$  are as derived in Equation (6) and  $f(x) = 0, g(x) = \mathbf{I}$  from (4). It is evident that for a given  $p_T$ , the constraint (8) is linear in  $u$ , so that the quadratic equation can be solved at high speeds, using the CVXPY library from python for convex optimization problems. Since square roots are present in the constraint equation, a discontinuity occurs when  $l = 0$ , when the UAV is perfectly aligned with the target. However, the nominal controller can be used directly over this region. The obtained safe control input,  $u_T^*$  is converted to the world frame using the relationship,  $u_W^* = \mathbf{R}^T u_T^*$ . Further, the yaw velocities are obtained as,

$$\dot{\psi}_d = K_\psi(\psi_d - \psi), \quad (9)$$

where  $K_\psi$  is a positive scalar and  $\psi_d$  is the desired yaw to establish the contact.

Now, the velocity tracking control and the lower level control are handled by the PX4's internal controller, to which we send the desired velocity inputs  $u_W^*, \dot{\psi}_d$ . Since the UAV is an underactuated system, there is a partial coupling between the position and attitude dynamics. The desired attitude commands are chosen from the desired thrust along different axes. The internal controller uses a first PID controller to obtain the desired forces to track the input velocities. Then, it obtains the upward thrust and desired attitude from these forces. Further, it uses two PID controllers to track the attitude and angular velocities.

### III. SYSTEM DESCRIPTION

This section is devoted to presenting the various subsystems crucial for the proper evaluation of the methodology outlined in Section II. To validate the proposed approach, an aerial manipulator platform is presented (Section III-A). The platform integrates an appropriate sensor setup for navigation and autonomous flight and a robotic arm for safe interaction with the environment. Another requirement for the validation of the approach is represented by the integration of target localization into the software architecture. The proposed solution for detecting target pose relies indeed on a Neural Network-based algorithm, which makes the integration with on-board computers not suitable for the proper performance of the Neural Network. To efficiently tackle this challenge, we have implemented an edge computing environment, which allows us to offboard the computation of *target detection* to a Kubernetes (k8s) clusters, as detailed in Section III-B.2. Furthermore, Section III-B.1 offers thorough insights into the communication aspects of the developed architecture, including communication within various subsystems onboard the drone and between the drone and *target detection* executed in the cluster.

#### A. Platform

For evaluating the proposed approach, a Tarot 650 served as the experimental platform. The drone is equipped with sensors to enable localization and secure interaction with the environment. Specifically, for target localization and detection, an *Intel RealSense D455* depth camera is integrated into the platform. This camera utilizes color and depth



images, that are required for marker detection, as detailed in Section III-B.1. Moreover, for precise target navigation, an *Intel RealSense T265* tracking camera and a *TF-mini* 1D LiDaR are incorporated repeatedly for pose and depth measurements. Additionally, for flight controller testing, a Pixhawk with the PX4 Flight stack was integrated. The comprehensive list of sensors is provided in Table I. To ensure safe interactions with contact surfaces when the target is reached, the flexible compliant arm introduced in [32] is integrated into the multirotor which enables the drone to perform physical interactions with the environment safely, without compromising its performance, due to its flexible properties and overall small weight.

Sensor Setup	
Components	Model
IMU	ICM-20948, ICM-20602 IMU
Color and Depth camera	Realsense D455
Tracking Camera	Realsense T265
1D LiDaR	TF Mini

TABLE I: Sensor setup integrated into Tarot T650 for experiments.

### B. Communication and Edge Offload

An inherent advantage of employing aerial robots for inspection lies in their ability to reduce costs and mitigate risks for human operators [33]–[35]. To further enhance cost-effectiveness, more affordable onboard computers are utilized. While many processes are executed on the onboard computer, the computational intensity of certain tasks necessitates offloading. Critical operations such as localization are executed on the onboard computer due to their time-sensitive nature. On the other hand, for tasks like target detection, which is crucial for successful inspections, an edge computing paradigm is employed to achieve optimal performance without introducing time delays [36]–[38]. This approach allows the execution of the resource-intensive neural network for target detection on a powerful edge computing system, leveraging heavy Graphics Processing Unit (GPU), preventing potential crashes on the onboard computer.

1) *Data Transmission*: In the proposed approach, data transmission for successful mission execution is divided into two layers (see Fig. 2). The first layer involves communication among Robot Operating System (ROS) nodes, both within the robot’s onboard computer and in the edge computing environment. The second layer, based on the principles outlined in [39], [40], utilizes a UDP tunnel for transmitting ROS messages as UDP packets. This transmission occurs via Wi-Fi or cellular networks, facilitating bidirectional communication from the robot to the edge and back. This method effectively addresses the inherent challenges of ROS communication between the internal cluster and the external cluster nodes.

2) *Edge Offloading*: The proposed approach utilizes an edge computing environment, leveraging a k8s cluster, to offload target detection algorithms. As illustrated in Fig. 2, the cluster processes camera data  $(x_i(k) \in \mathbb{Z}^{n \times m}$ , where

$n \times m$  represents the image matrix size, at time step  $k$ ) received from the robot and generating target localization  $(u_i(k) \in \mathbb{R}^{1 \times 3})$  relative to the global frame. The system, however, encounters uplink ( $d_1 \in \mathbb{R}^+$ ) and downlink ( $d_2 \in \mathbb{R}^+$ ) delays. A filtering method is introduced to ensure accurate target localization; it disregards the localization output when the round-trip-time (RRT) for the closed-loop system exceeds the maximum threshold  $\tau^{max}$ . Then, the operation of the system can be expressed as

$$u_i(k) = \begin{cases} f(x_i(k + d_1)), & \text{if } d_1 + d_2 \leq \tau^{max} \\ \text{“ignore”}, & \text{otherwise} \end{cases} \quad (10)$$

where  $f(\cdot)$  is the target detection function executed in the edge computing environment.

The condition  $d_1 + d_2 \leq \tau^{max}$  ensures that the target localization is only considered if the communication delay is within acceptable limits. If the delays exceed  $\tau^{max}$ , the target localization is disregarded to avoid using outdated or inaccurate data.

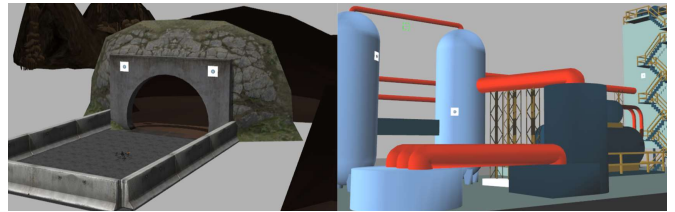
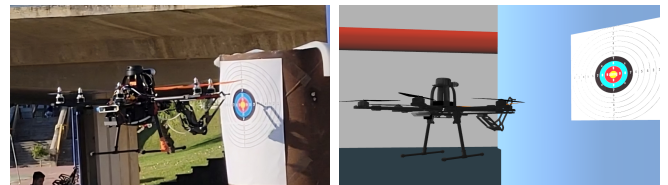


Fig. 7: Simulation environments for the evaluation of the proposed architecture. Including tunnel (left) and refinery plant (right).



(a) Real platform in industrial (b) Platform in Gazebo simulation environment

Fig. 8: Side to side comparison of real and simulated UAV.

## IV. EXPERIMENTAL APPLICATIONS

The following section is devoted to the evaluation of the capabilities of the presented approach. In particular, Section IV-A is devoted to the discussion of the results obtained in the Simulation environment, while Section IV-B focuses on the experimental results obtained in real time.

### A. System Evaluation

Along with the prototype, an advanced simulation environment has been designed, taking into account the aerial manipulator prototype, the sensor setup, and realistic world environments. The simulated version of the prototype is then incorporated into the Gazebo Simulator, following the procedure introduced in [41], and into PX4 Software in the Loop (SITL) software for the testing phase (see Fig. 7). The simulated version includes a model of all the sensors

integrated into the prototype (Table I) as well as an estimate of the mass and inertia of all components. A representation of the platform in simulation is presented in Fig. 8b. The development of the Simulator allows us to test the whole architecture in different simulation scenarios to evaluate the performance and robustness of the proposed solution. In particular, the experiments in the Simulation environment are performed in two different scenarios, introduced in [42] and [43], to evaluate the behavior of the system under different light and environmental conditions (see Fig. 8).

The performance of the controller is validated in the simulated environments, which is highlighted in Fig. 9 - 12. In the simulated scenario, the controller is commanded to precisely navigate the UAV to the given target's pose (obtained from the target detection framework). Fig. 9 visualizes how the CBF sets a boundary (red mesh) for the UAV to maneuver safely towards the target without requiring an external planner, where run 1 corresponds to the cave environment, and run 2 corresponds to the refinery environment. It is to be noted that the mesh and the position error trajectories ( $e_x, e_y, e_z$  in Fig. 9, 11) are the same as the position trajectories of the UAV in the target frame ( $x_D^T, y_D^T, z_D^T$ ). In run 1, though the UAV starts from an unsafe region, the trajectory converges to the safe zone and approaches the target through it. The action of the CBF is further evident from Fig. 11, where the error trajectories  $e_y, e_z$  converge to zero much faster than  $e_x$ , showing that the UAV aligns itself right in front of the target before approaching it and hence forming a parabolic trajectory as seen in Fig. 9. Further, in Fig. 10, the asymptotic convergence to the safe zone, while starting from an unsafe zone is evident in Run 1, where the  $h$  value starts from a negative value and rapidly increases to a positive value. When a positive value is reached, it approaches the target horizontally. After around 12 seconds, the values of  $h$  in both trajectories get close to zero when the UAV gets close to the target, where the safe region narrows into a point. It can be observed that there are steep changes in the commanded control inputs in Fig. 12, as the CBF tries to push the UAV to remain in the safe zone. However, due to the actuator's physical limitations, the UAV gets into the unsafe zone momentarily. So, the  $h$  values, and hence the commanded velocities slowly oscillate near the target to maintain the position error as close as possible to zero, which is observed in Fig. 11. When the UAV reaches the tip of the funnel, it establishes contact with the target safely with a very low velocity.

### B. Target Detection Evaluation

The validation of the detection algorithm was conducted across various scenarios, each characterized by distinct lighting and environmental conditions, facilitating a comprehensive assessment of the proposed approach's performance and robustness. In particular, experiments were conducted in three different locations: a parking lot, a tunnel, and an outdoor environment during midday with intense sunlight. Each location presented unique challenges, allowing for a thorough evaluation of target detection performance. Visual testing

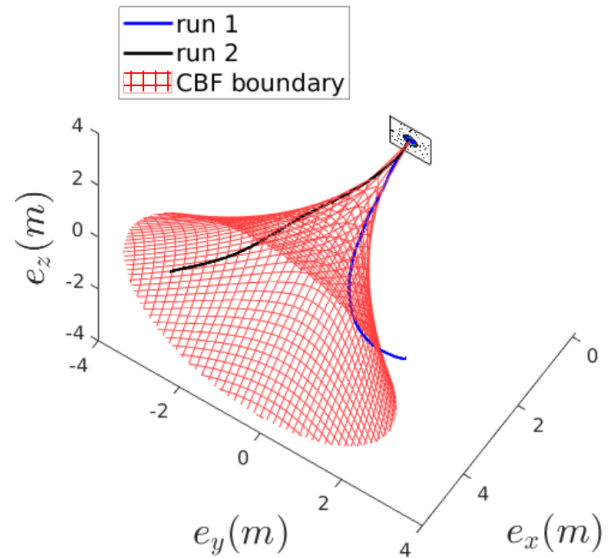


Fig. 9: The CBF boundary layer ( $a = 3$ ) along with the trajectories of the UAV guided by the CBF to the target.

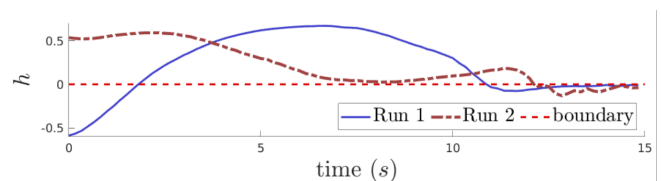


Fig. 10: The values of  $h$  during Run 1 and Run 2.

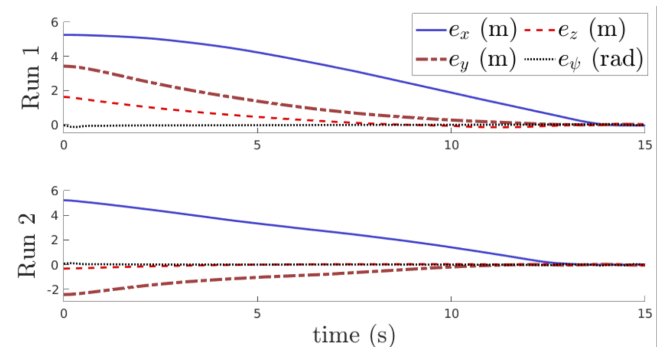


Fig. 11: Errors in position and yaw of the UAV for the two runs.

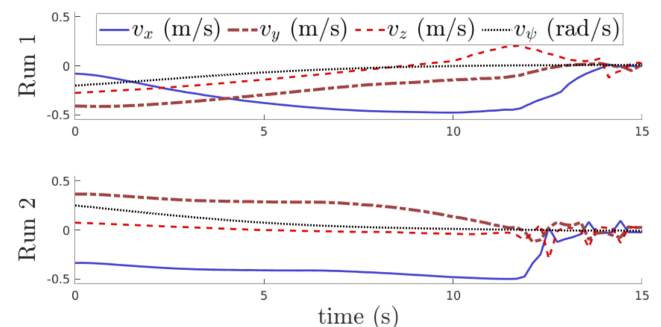


Fig. 12: Commanded velocity for the UAV for the runs.

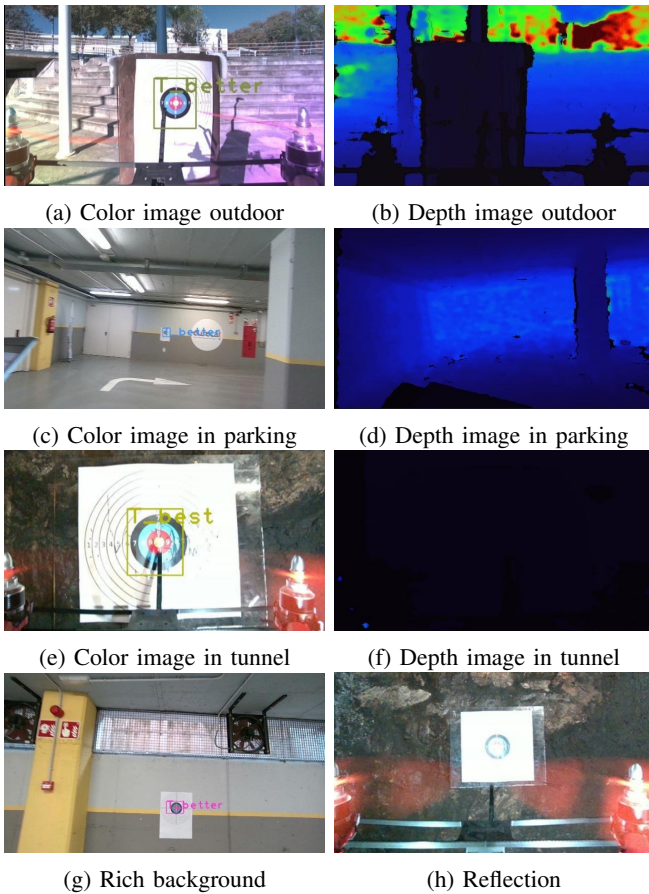


Fig. 13: Color and depth images of target detection in real flight application with previously unseen images.

was performed during each flight, and Fig. 13 illustrates three samples showcasing the detector’s output alongside depth images. From the image, it’s possible to notice the different light conditions that affect the color and depth: the first and second scenarios are particularly dark, as evidenced by the lack of discernible information in the depth images. Additionally, the second scenario posed additional challenges due to reflections generated by the target cover, Fig. 13h. In contrast, the third scenario presents contrasting conditions with ample sunlight, resulting in potential overexposure of the image sensor and a resulting pink hue in the images.

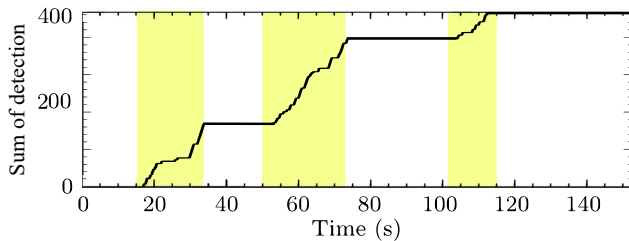


Fig. 14: Plot of the sum of target detection through time during a flight test. Regions in yellow highlight moments when a target is within the camera’s field of view.

Despite the different conditions faced, the detector consistently demonstrated robust performance, achieving  $T_{best}$

performance label detection even with a scratched target (see Fig. 13e), and  $T_{better}$  in long-distance estimation (see Fig. 13c). This last detection is also impressive due to the proximity of a spherical pattern that could have been detected as a false positive. Fig. 13g also shows the detection quality in a rich features environment. Nevertheless, it is interesting to notice that light reflections on the target surface in the tunnel lead to false negative detection.

Due to the onboard computer’s inability to process data, execute the detection algorithm, and determine the target’s location in real time, we employed the edge offloading strategy. Camera data were streamed to the k8s cluster for target detection and localization. Subsequently, the target’s location was transmitted to the aerial platform for its navigation.

To further evaluate the algorithm’s performance, we conducted additional experiments in the tunnel, which is the most demanding environment. The test consists of a flight with multiple fly-bys to different targets attached to the walls. We evaluate the number of positive target detections during the all flight. The result is presented in Figure 14. It shows that whenever a target enters the field of view, there is an increase in the number of target detections. Conversely, this count remains constant when the target exits the camera’s field of view, showing consistency of true negatives.

Overall, the behavior of the algorithm and the quality of detection exhibit robustness and consistency across various flight tests and scenarios. The algorithm consistently demonstrates strong performance, successfully detecting targets with reliability regardless of the environmental conditions or flight scenarios encountered.

## V. CONCLUSIONS AND FUTURE WORK

In this work, we introduced a refined approach to autonomously and safely engage with a target, blending neural networks with traditional control methods. By leveraging deep learning solely for image processing and maintaining a model-based planner and controller, we ensured precise control outputs. Utilizing edge computing, we offloaded the computationally intensive neural tasks requiring a GPU, preserving the lightweight nature of the MAV while ensuring mission oversight. Furthermore, employing an onboard CBF-based controller enables the UAV to navigate safely and accurately establish contact with the target without relying on an external planner. Experimental validation of the system underscored the effectiveness of the proposed architecture.

Future steps will include the evaluation of the whole architecture in the real world and the integration of the exploration phase, to enable UAV to autonomously conduct scheduled, and safe APhI tasks in industrial environments.

## REFERENCES

- [1] A. Ollero and B. Siciliano, *Aerial robotic manipulation*. Springer, 2019.
- [2] G. Nikolakopoulos, S. S. Mansouri, and C. Kanellakis, *Aerial Robotic Workers: Design, Modeling, Control, Vision and Their Applications*. Butterworth-Heinemann, 2022.
- [3] A. Ollero, M. Tognon, A. Suarez, D. Lee, and A. Franchi, “Past, present, and future of aerial robotic manipulators,” *IEEE Transactions on Robotics*, vol. 38, no. 1, pp. 626–645, 2022.

- [4] A. Viguria, R. Caballero, Á. Petrus, F. J. Pérez-Grau, and M. Á. Trujillo, "Aerial robotic system for complete bridge inspections," in *Advances in Road Infrastructure and Mobility*. Cham: Springer International Publishing, 2022, pp. 171–186.
- [5] Y. Zhu, J. Zhou, Y. Yang, L. Liu, F. Liu, and W. Kong, "Rapid target detection of fruit trees using uav imaging and improved light yolov4 algorithm," *Remote Sensing*, vol. 14, no. 17, p. 4324, 2022.
- [6] Y. Li, H. Yuan, Y. Wang, and C. Xiao, "Ggt-yolo: A novel object detection algorithm for drone-based maritime cruising," *Drones*, vol. 6, no. 11, 2022. [Online]. Available: <https://www.mdpi.com/2504-446X/6/11/335>
- [7] Z. Xiao, F. Wan, G. Lei, Y. Xiong, L. Xu, Z. Ye, W. Liu, W. Zhou, and C. Xu, "Fl-yolov7: A lightweight small object detection algorithm in forest fire detection," *Forests*, vol. 14, no. 9, 2023. [Online]. Available: <https://www.mdpi.com/1999-4907/14/9/1812>
- [8] J. Sun, B. Li, Y. Jiang, and C.-y. Wen, "A camera-based target detection and positioning uav system for search and rescue (sar) purposes," *Sensors*, vol. 16, no. 11, 2016. [Online]. Available: <https://www.mdpi.com/1424-8220/16/11/1778>
- [9] P. Jiang, D. Ergu, F. Liu, Y. Cai, and B. Ma, "A review of yolo algorithm developments," *Procedia Computer Science*, vol. 199, pp. 1066–1073, 2022.
- [10] M. Kou, L. Zhou, J. Zhang, and H. Zhang, "Research advances on object detection in unmanned aerial vehicle imagery," *Meas. Control. Technol.*, vol. 39, pp. 47–61, 2020.
- [11] L. Tan, X. Lv, X. Lian, and G. Wang, "Yolov4\_drone: Uav image target detection based on an improved yolov4 algorithm," *Computers & Electrical Engineering*, vol. 93, p. 107261, 2021. [Online]. Available: <https://www.sciencedirect.com/science/article/pii/S0045790621002445>
- [12] P. Pradeepkumar, A. Pal, and K. Kant, "Resource efficient edge computing infrastructure for video surveillance," *IEEE Transactions on Sustainable Computing*, pp. 1–1, 2021.
- [13] C. O. Bitey Dimithe, C. Reid, and B. Samata, "Offboard machine learning through edge computing for robotic applications," in *South-eastCon 2018*, 2018, pp. 1–7.
- [14] S. Ganguly, V. N. Sankaranarayanan, B. Suraj, R. D. Yadav, and S. Roy, "Efficient manoeuvring of quadrotor under constrained space and predefined accuracy," in *2021 IEEE/RSJ International Conference on Intelligent Robots and Systems (IROS)*. IEEE, pp. 6352–6357.
- [15] V. N. Sankaranarayanan, R. D. Yadav, R. K. Swayampakula, S. Ganguly, and S. Roy, "Robustifying payload carrying operations for quadrotors under time-varying state constraints and uncertainty," *IEEE Robotics and Automation Letters*, vol. 7, no. 2, pp. 4885–4892, 2022.
- [16] V. N. Sankaranarayanan, S. Satpute, S. Roy, and G. Nikolakopoulos, "Adaptive control of euler-lagrange systems under time-varying state constraints without a priori bounded uncertainty," *IFAC-PapersOnLine*, vol. 56, no. 2, pp. 3360–3365, 2023.
- [17] A. D. Ames, S. Coogan, M. Egerstedt, G. Notomista, K. Sreenath, and P. Tabuada, "Control barrier functions: Theory and applications," in *2019 18th European control conference (ECC)*. IEEE, 2019, pp. 3420–3431.
- [18] A. Saviolo and G. Loianno, "Learning quadrotor dynamics for precise, safe, and agile flight control," *Annual Reviews in Control*, vol. 55, pp. 45–60, 2023. [Online]. Available: <https://www.sciencedirect.com/science/article/pii/S1367578823000135>
- [19] A. Ollero and B. Siciliano, *Aerial Robotic Manipulation*. Springer, 2019.
- [20] N. O'Mahony, S. Campbell, A. Carvalho, S. Harapanahalli, G. V. Hernandez, L. Krpalkova, D. Riordan, and J. Walsh, "Deep learning vs. traditional computer vision," in *Advances in Computer Vision: Proceedings of the 2019 Computer Vision Conference (CVC), Volume 1 I*. Springer, 2020, pp. 128–144.
- [21] W. Qing, H. Chen, X. Wang, and Y. Yin, "Collision-free trajectory generation for uav swarm formation rendezvous," in *2021 IEEE International Conference on Robotics and Biomimetics (ROBIO)*. IEEE, 2021, pp. 1861–1867.
- [22] H. Lee, S. Jung, and D. H. Shim, "Vision-based uav landing on the moving vehicle," in *2016 International conference on unmanned aircraft systems (ICUAS)*. IEEE, 2016, pp. 1–7.
- [23] M. Lippi and A. Marino, "A control barrier function approach to human-multi-robot safe interaction," in *2021 29th Mediterranean Conference on Control and Automation (MED)*. IEEE, 2021, pp. 604–609.
- [24] F. Ferraguti, M. Bertuletti, C. T. Landi, M. Bonfè, C. Fantuzzi, and C. Secchi, "A control barrier function approach for maximizing performance while fulfilling to iso/ts 15066 regulations," *IEEE Robotics and Automation Letters*, vol. 5, no. 4, pp. 5921–5928, 2020.
- [25] J. Liang, H. Zhong, Y. Wang, Y. Chen, J. Zeng, and J. Mao, "Adaptive force tracking impedance control for aerial interaction in uncertain contact environment using barrier function," *IEEE Transactions on Automation Science and Engineering*, 2023.
- [26] H.-Y. Lin and J.-R. Zhan, "Gnss-denied uav indoor navigation with uwb incorporated visual inertial odometry," *Measurement*, vol. 206, p. 112256, 2023.
- [27] H. Luo, G. Li, D. Zou, K. Li, X. Li, and Z. Yang, "Uav navigation with monocular visual inertial odometry under gnss-denied environment," *IEEE Transactions on Geoscience and Remote Sensing*, vol. 61, pp. 1–15, 2023.
- [28] "Visual Inertial Odometry (VIO) — PX4 User Guide (v1.12)." [Online]. Available: [https://docs.px4.io/v1.12/en/computer\\_vision/](https://docs.px4.io/v1.12/en/computer_vision/)
- [29] M. Fiala, "Designing highly reliable fiducial markers," *IEEE Transactions on Pattern Analysis and Machine Intelligence*, vol. 32, no. 7, pp. 1317–1324, 2010.
- [30] K. Wada, "wktentaro/labelme," Nov. 2021. [Online]. Available: <https://doi.org/10.5281/zenodo.5711226>
- [31] E. Marchand, H. Uchiyama, and F. Spindler, "Pose estimation for augmented reality: a hands-on survey," *IEEE transactions on visualization and computer graphics*, vol. 22, no. 12, pp. 2633–2651, 2015.
- [32] J. Mellet, A. Berra, A. Santi Seisa, V. Sankaranarayanan, U. Gamage, M. Trujillo, G. Heredia, G. Nikolakopoulos, V. Lippiello, and F. Ruggiero, "Design of a flexible robot arm for safe aerial physical interaction," in *2024 IEEE 7th International Conference on Soft Robotics (RoboSoft)*. IEEE, 2024.
- [33] M. Bobbe, Y. Khedar, J. Backhaus, M. Gerke, Y. Ghassoun, and F. Plöger, "Reactive mission planning for uav based crane rail inspection in an automated container terminal," in *2020 International Conference on Unmanned Aircraft Systems (ICUAS)*, 2020, pp. 1286–1293.
- [34] R. S. Pahwa, K. Y. Chan, J. Bai, V. B. Saputra, M. N. Do, and S. Foong, "Dense 3d reconstruction for visual tunnel inspection using unmanned aerial vehicle," in *2019 IEEE/RSJ International Conference on Intelligent Robots and Systems (IROS)*, 2019, pp. 7025–7032.
- [35] S. S. Mansouri, C. Kanellakis, E. Fresk, D. Kominaki, and G. Nikolakopoulos, "Cooperative uavs as a tool for aerial inspection of the aging infrastructure," in *Field and Service Robotics: Results of the 11th International Conference*. Springer, 2017, pp. 177–189.
- [36] S. Liang, H. Wu, L. Zhen, Q. Hua, S. Garg, G. Kaddoum, M. M. Hassan, and K. Yu, "Edge yolo: Real-time intelligent object detection system based on edge-cloud cooperation in autonomous vehicles," *IEEE Transactions on Intelligent Transportation Systems*, vol. 23, no. 12, pp. 25 345–25 360, 2022.
- [37] Q. Cheng, H. Wang, B. Zhu, Y. Shi, and B. Xie, "A real-time uav target detection algorithm based on edge computing," *Drones*, vol. 7, no. 2, p. 95, 2023.
- [38] M. S. Alam, B. Natesha, T. Ashwin, and R. M. R. Guddeti, "Uav based cost-effective real-time abnormal event detection using edge computing," *Multimedia tools and Applications*, vol. 78, pp. 35 119–35 134, 2019.
- [39] G. Damigos, N. Stathoulopoulos, A. Koval, T. Lindgren, and G. Nikolakopoulos, "Communication-aware control of large data transmissions via centralized cognition and 5g networks for multi-robot map merging," *Journal of Intelligent & Robotic Systems*, vol. 110, no. 1, p. 22, 2024.
- [40] G. Damigos, A. S. Seisa, S. G. Satpute, T. Lindgren, and G. Nikolakopoulos, "A resilient framework for 5g-edge-connected uavs based on switching edge-mpc and onboard-pid control," in *2023 IEEE 32nd International Symposium on Industrial Electronics (ISIE)*. IEEE, 2023, pp. 1–8.
- [41] A. Berra, P. J. Sanchez-Cuevas, M. Trujillo, G. Heredia, and A. Viguria, "Airframe - fast prototyping framework for uavs definition," in *2023 International Conference on Unmanned Aircraft Systems (ICUAS)*, 2023, pp. 1175–1182.
- [42] L. Markovic, F. Petric, A. Ivanovic, J. Goricanec, M. Car, M. Orsag, and S. Bogdan, "Towards a standardized aerial platform: ICUAS'22 firefighting competition," *Journal of Intelligent Robotic Systems*, vol. 108, no. 3, Jul. 2023. [Online]. Available: <https://doi.org/10.1007/s10846-023-01909-z>



- [43] A. Koval, C. Kanellakis, E. Vidmark, J. Haluska, and G. Nikolakopoulos, "A subterranean virtual cave world for gazebo based on the darpa subt challenge," *arXiv preprint arXiv:2004.08452*, 2020.